High Power Laser Science and Engineering, (2025), Vol. 13, e69, 10 pages.
doi:10.1017/hpl.2025.10033

HIGH POWER LASER SCIENCE AND ENGINEERING

RESEARCH ARTICLE

B-integral limitation of ultra-high-peak-power lasers

Zhaoli Li, Kainan Zhou, Jie Mu, Xiaoming Zeng, Zhaohui Wu, Xiao Wang, Xiaodong Wang, and Yanlei Zuo

National Key Laboratory of Plasma Physics, Laser Fusion Research Center, China Academy of Engineering Physics, Mianyang, China

(Received 15 January 2025; revised 25 March 2025; accepted 29 April 2025)

Abstract

In the design and construction of ultra-high-peak-power laser systems, it is necessary to control the accumulated B-integral of the laser pulse, but currently there are no reasonable B-integral control standards for picosecond and femtosecond lasers. We systematically evaluate the influence of the B-integral on the output capability of picosecond and femtosecond laser systems for the first time, to our knowledge, taking Nd:glass lasers and Ti:sapphire lasers as examples. For picosecond lasers, the temporal domain compressibility and the small-scale self-focusing effect restrict the B-integral to 1.7 and 1.9, respectively. For femtosecond lasers, the B-integral is mainly restricted by the small-scale self-focusing effect and the far-field focusability, which limit the B-integral to 1.5 and 1.7, respectively. The restriction made by far-field focusability can be largely relaxed by inserting a deformable mirror. The study of the factors restricting the B-integral will provide guidance for the design of ultra-high-peak-power laser systems.

Keywords: B-integral; self-phase modulation; small-scale self-focusing; Strehl ratio; ultra-high-peak-power lasers

1. Introduction

Since the advent of lasers, enhancing the laser intensity has been one of the goals pursued in the development of laser technology. Over the past few decades, thanks to the development of chirped pulse amplification (CPA) technology[1], advanced laser gain media and high-power solid-state laser technologies, the peak power of laser devices has achieved a leapfrog development. Currently, several large-scale laser systems have been built or are under construction worldwide. These systems can generate laser pulses with widths as short as the picosecond and femtosecond scale, capable of delivering petawatt-level laser pulses, with a focused power density reaching the 10^{23} W/cm^2[2] level. Such high laser power density can create unprecedented extreme physical conditions in the laboratory, providing a technical foundation and tools for many cutting-edge scientific researches, thus giving birth to the new field of strong-field physics and many interdisciplinary studies, which have become a hot topic of widespread attention and active exploration in the international academic community.

From the perspective of technical characteristics and application backgrounds, the development of ultra-intense laser technology has formed two main branches. One is the high-energy picosecond pulse laser with neodymium glass as the amplification medium, and the other is the high-peak-power femtosecond pulse laser with titanium-doped sapphire as the amplification medium. The former is mainly aimed at research needs in fields such as laser fusion, high-energy-density physics and materials science, while the latter is suitable for the study of strong-field physics and other fields with faster time processes. In the field of high-energy picosecond pulse lasers, the Lawrence Livermore National Laboratory (LLNL) built the world's first picosecond petawatt laser device, named Petawatt[3], in May 1996, driven by the demand for inertial confinement fusion (ICF) ignition research. In the following decades, several picosecond petawatt laser devices, such as Vulcan[4], Gekko-XII[5], NIF-ARC[6], Texas Petawatt Laser[7] and PETAL[8], were successively built in various countries. The experiments conducted on these devices have greatly enriched people's understanding of laser fusion, high-energy-density physics and other fields.

Titanium-doped sapphire has a gain bandwidth of 230 nm, a saturation flux of 1 J/cm^2 and a high thermal conductivity, making it an ideal medium for high-peak-power, high-repetition-rate femtosecond laser pulses. The BELLA device

Correspondence to: Y. Zuo, National Key Laboratory of Plasma Physics, Laser Fusion Research Center, China Academy of Engineering Physics, Mianyang 621900, China. Email: zuoyanlei@tsinghua.org.cn

built in Berkeley in 2013 is the world's first petawatt laser based on titanium sapphire[9]. After amplification through multiple CPA amplifiers and Ti:sapphire amplifiers, this device can output a single pulse energy of more than 40 J, with a pulse width of less than 30 fs, a peak power of 1.3 PW and a repetition rate of 1 Hz. Since then many Ti:sapphire laser systems, such as CoReLS[10], SULF[11] and HPLS[12], have been built worldwide. In addition, based on the full-chain optical parametric chirped pulse amplification (OPCPA) scheme, the Laser Fusion Research Center of the China Academy of Engineering Physics successfully developed the SILEX-II device in 2017[13], which can produce a laser pulse of 91.1 J and 18.6 fs, with a peak power of 4.9 PW. Currently, many countries and organizations are striving towards the goal of 100 PW lasers[14].

In the design and construction of ultra-short and ultra-intense laser systems, the control of the B-integral is a key factor that needs to be considered. In the time domain, the introduction of the B-integral leads to the generation of high-order dispersion, which affects the accurate compensation of second-, third- and fourth-order dispersion by the gratings, which are designed for compensating the material dispersion, resulting in an increase of the pulse width after compression and a decrease of the peak intensity since, for a certain level of the B-integral, effective compression is impossible. In the spatial domain, on the one hand, the introduction of the B-integral causes different wavefront phase distortions at different spatial positions of the laser pulse, thereby affecting the far-field focusability of the laser pulse; on the other hand, the small-scale self-focusing effect (SSSF), whose growth rate is proportional to the B-integral, amplifies the spatial modulation in the near-field of the laser pulse, leading to a decrease in near-field quality or even damage to optical elements. For high-energy nanosecond laser systems, experience suggests that the B-integral should be controlled within 2–3[15–18]. In the National Ignition Facility (NIF), the B-integral of one-stage amplification is controlled to be less than 1.8[15], and the total cumulative B-integral of all stages is controlled to be less than 3.5[16]. At the same time, deformable mirrors, spatial filters and other methods are used to suppress the phase and amplitude modulation in the laser pulse. For broadband laser systems, some researchers suggested that the B-integral should be controlled to far less than 1[19], but there is currently a lack of systematic research on the rigorous B-integral criterion. In this paper, we calculate the changes in the temporal domain compressibility, the near-field modulation and the far-field focusability of chirped laser pulses under the influence of different B-integrals and, based on this, provide a strict criterion for the B-integral. Section 2 discusses the impact of the B-integral on the compression ability of chirped lasers. Section 3 discusses the near-field modulation caused by the SSSF related to the B-integral. Section 4 discusses the influence of the B-integral on the laser focusing capability. Section 5 provides the conclusion.

2. Impact of the B-integral on the compression ability of chirped lasers

Ultra-high-peak-power lasers are typically generated through CPA/OPCPA technology. In this process, a low-energy broadband seed pulse is first stretched into a nanosecond pulse by a stretcher. Subsequently, the nanosecond pulse is amplified through several pieces of gain media or parametric crystals, and then compressed to its minimum pulse width using a compressor. During this process, the nanosecond laser pulse with a certain chirp passes through multiple transmission elements. Each time it passes through a transmission element, a nonlinear phase shift accumulates due to the nonlinear refractive index of the transmission medium, which is given by the B-integral $B = \sum \omega_0 n_2 I_0 L/c$, where ω_0 is the laser frequency, c is the speed of light, I_0 is the laser intensity, n_2 is the nonlinear refractive index of the medium and L is the length of the medium. Since this nonlinear phase shift is related to the intensity, the local frequency at each position of the laser pulse will change and new frequency elements will be generated, which is known as self-phase modulation (SPM). SPM disrupts the linear chirp of the laser pulse, generating higher-order dispersion, making it impossible for the compressor to compress the laser to its minimum pulse width. Therefore, in short-pulse laser systems, considering the impact of the spectral phase, it is necessary to control the B-integral accumulated during the amplification process of the laser pulse.

Assuming that the laser pulse has a certain chirp after passing through the stretcher and a B-integral is introduced during the amplification process, then before entering the compressor, the temporal waveform of the laser can be written as follows:

$$E(t) = E_0 \exp\left(-(1+iC)\frac{t^2}{2T_p^2} + iB\exp\left(-\frac{t^2}{T_p^2}\right)\right). \quad (1)$$

Here, E_0 represents the peak laser intensity, C is the coefficient of the chirp rate, $T_p = T_h/\sqrt{4\ln 2}$ is the $1/e$ pulse width of the chirped laser intensity and T_h is the full width at half maximum of the laser intensity. The relationship between T_h and C is as follows: $\Delta\omega T_h/2\pi = 0.441\sqrt{1+C^2}$, where $\Delta\omega = 2\pi c\Delta\lambda/\lambda_0^2$ is the spectral width (full width at half maximum) of the laser pulse, $\lambda_0 = 2\pi c/\omega_0$ is the central wavelength of the laser and $\Delta\lambda$ is the bandwidth (full width at half maximum) of the laser. In experiments, a more commonly used quantity is the chirp amount D, which is defined as the ratio of the laser's full width at half maximum to its bandwidth: $D = T_h/\Delta\lambda = 0.441\sqrt{1+C^2}\lambda_0^2/c(\Delta\lambda)^2$.

https://doi.org/10.1017/hpl.2025.10033 Published online by Cambridge University Press

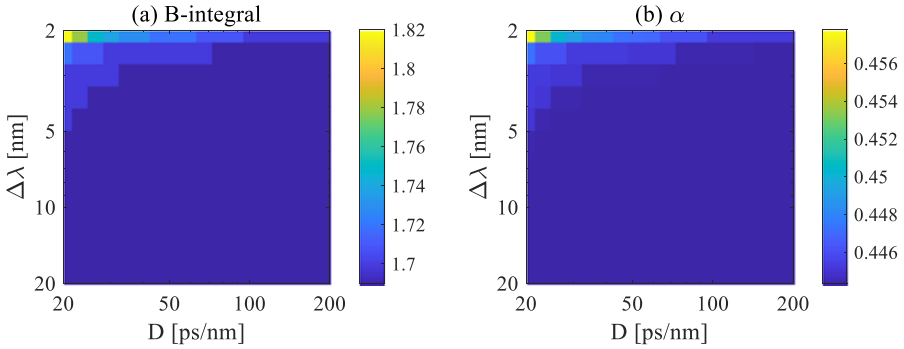

Figure 1. For Gaussian pulses, (a) the maximum tolerable B-integral and (b) the corresponding α value when the laser pulse has different bandwidths and different chirp amounts.

Taking the derivative of the phase term, the instantaneous frequency at each position of the laser pulse is obtained as follows:

$$\omega = \frac{t}{T_p^2}\left(C + 2B\exp\left(-\frac{t^2}{T_p^2}\right)\right). \tag{2}$$

Performing a Taylor expansion of the B-integral term in the laser waveform:

$$E(t) = E_0 e^{iB}\exp\left(-\frac{t^2}{2T_p^2} - i(C+2B)\frac{t^2}{2T_p^2} + iB\frac{t^4}{T_p^4} + \cdots\right). \tag{3}$$

Its Fourier transform is approximately given by the following:

$$\tilde{E}(\omega) \approx \tilde{E}_{0\omega}\exp\left(-\frac{T_p^2}{1+i(C+2B)}\frac{\omega^2}{2} + iB\frac{6T_p^4}{(1+i(C+2B))^4}\frac{\omega^4}{24} + \cdots\right). \tag{4}$$

When the B-integral is neglected, adjusting the compression grating to compensate for the second-order dispersion $\mathrm{GDD} = -\frac{CT_p^2}{1+C^2}$ can minimize the pulse width of the output pulse. When the intensity increases, if no additional compensation is made by moving the compression grating under a certain B-integral, the pulse width of the output pulse will be broadened at high laser energy. Considering a chirped laser pulse with a central wavelength of 1000 nm, we calculated the B-integral corresponding to the decrease of the compressed laser peak intensity to 90% under different laser bandwidths and chirp amounts. We found that within a wide range of laser bandwidths and chirp amounts ($\Delta\lambda$ = 5–50 nm, D = 10–500 ps/nm), when the B-integral reaches approximately 0.96, the laser intensity drops to 90%. It can be seen that if the grating is set at low energy and no adjustment was made at high energy (for example, in single-shot lasers), the B-integral should be designed to be less than 1.

However, in experiments, we can often achieve a more ideal compression effect by fine-tuning the spacing of the compression grating to compensate for the additional second-order dispersion induced by the B-integral. We assume that the additional second-order dispersion required to compress the high-energy laser to the limit pulse width is $\mathrm{GDD}' = \alpha B\frac{T_p^2}{1+C^2}$, where α is an adjustable parameter. The B-integral corresponding to the decrease of the compressed laser peak intensity to 90% and the corresponding α values under different laser bandwidths and chirp amounts are shown in Figure 1. It can be seen that when the laser bandwidth and chirp amount are small, the tolerable B-integral is high. When the laser bandwidth or chirp amount increases ($\Delta\lambda > 4$ nm, $D > 20$ ps/nm), the tolerable B-integral gradually drops to a fixed value of approximately 1.7, and the corresponding α value gradually stabilizes at around 0.444. It can be seen that if the second-order dispersion can be fine adjusted, it is only necessary to control the B-integral to be less than 1.7.

For picosecond lasers, it is reasonable to assume that their spectrum follows a Gaussian function. However, for femtosecond lasers with broader spectral widths, the laser spectra are often shaped to approximate a rectangular distribution through spectral shaping techniques. In this case, after passing through a stretcher, the temporal waveform of the laser pulse is also similar to rectangular distribution. Under such circumstances, the introduction of the B-integral does not generate new frequencies in the central part of the pulse because the strength of the SPM effect is related to the gradient of the laser intensity. Therefore, the influence of the B-integral induced during the amplification process on the compressed femtosecond lasers should be weakened. To verify this, we consider a chirped laser pulse with an n_{SG}-order super-Gaussian distribution in the frequency domain: $\tilde{E}(\omega) = \tilde{E}_0\exp\left(-\frac{\ln(2)}{2}\left(2\frac{\omega-\omega_0}{\Delta\omega}\right)^{2n_{SG}} + i\frac{\mathrm{GDD}}{2}(\omega-\omega_0)^2\right)$. Firstly, the value of GDD is estimated using the analytical formula in Gaussian light, but this value is not applicable to super-Gaussian light. Therefore, the value of GDD needs

https://doi.org/10.1017/hpl.2025.10033 Published online by Cambridge University Press

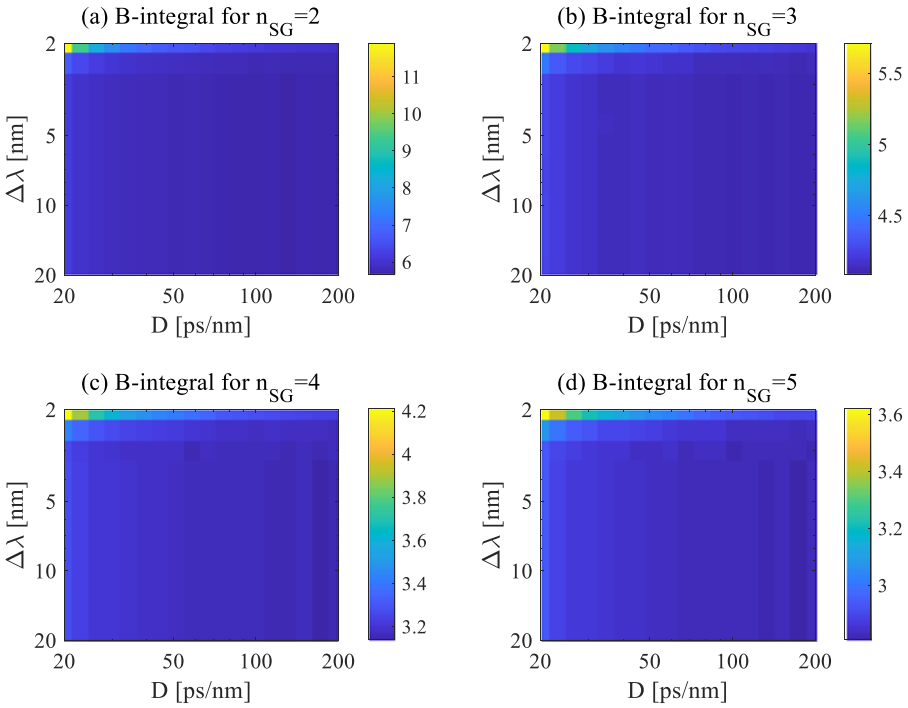

Figure 2. For super-Gaussian pulses with (a) $n_{SG} = 2$, (b) $n_{SG} = 3$, (c) $n_{SG} = 4$ and (d) $n_{SG} = 5$, the maximum tolerable B-integral when the laser pulse has different bandwidths and different chirp amounts.

to be finely adjusted so that the inverse Fourier transform of $\widetilde{E}(\omega)$ has a specified full width at half maximum $T_h = D\Delta\lambda$ in the time domain. Then, a certain B-integral is added to the laser pulse in the time domain, and the second-order dispersion GDD' required to compress the laser to the shortest width and the corresponding laser intensity are recalculated. For a super-Gaussian laser pulse, when the laser intensity decreases to 90%, the corresponding B-integral is taken as the maximum tolerable B-integral. When the laser pulse has different bandwidths $\Delta\lambda$ and chirp amounts D, the maximum tolerable B-integrals for $n_{SG} = 2$, 3, 4 and 5 are as shown in Figures 2(a)–2(d), respectively. It can be seen that for second-order super-Gaussian laser pulse, when the chirp amount and the bandwidth of the laser pulse are large enough, because of the central region of the laser's temporal waveform becoming flatter, the tolerable B-integral will be much higher than that of a Gaussian pulse and will finally stabilize at around 5.72. However, for third-, fourth- and fifth-order super-Gaussian pulses, the tolerable B-integral decreases to around 4.11, 3.16 and 2.83, respectively. This is because for a high-order super-Gaussian pulse, the edges of the laser are steeper and the high-order dispersions generated at the laser edges are unable to be compensated by the compressor. Therefore, a large amount of energy at the laser edges is wasted, which leads to the decrease of the maximum B-integral.

In femtosecond laser systems, an AOPDF (acousto-optic programmable dispersive filter) is commonly used to compensate dispersion up to the fifth order. In this configuration, the fourth-order dispersion induced by the B-integral can also be compensated within the compensation range. In the simulations, we found that within the parameter range of interest, the fourth-order dispersion generated by the B-integral typically far exceeds the compensation capability of the AOPDF (100,000 fs^4). Therefore, we do not consider the scenario where the fourth-order dispersion induced by the B-integral is fully compensated by the AOPDF in this study.

3. Small-scale self-focusing effect caused by the B-integral

In addition to causing high-order dispersion in the time domain, the introduction of the B-integral also leads to modulation instability of the laser pulse in the spatial domain, that is, small-scale self-focusing. Small-scale self-focusing often imposes stricter requirements on the B-integral, which will be discussed through the Bespalov-Talanov (B-T) theory[20]. The surface quality of optical elements can be described by the power spectral density (PSD), which is defined as the square of the amplitude of the Fourier elements of the surface undulation of the element:

$$S_{ph}(k_x) = \frac{\left(\int z(x)\exp(-ik_x x)\,dx\right)^2}{\Delta k_x}. \quad (5)$$

For amplitude noise, $z(x)$ is the transmitted/reflected laser amplitude at each measurement point; for phase noise, $z(x)$

https://doi.org/10.1017/hpl.2025.10033 Published online by Cambridge University Press

is the measured thickness at each measurement point. Here, we only consider phase noise. For phase noise, the PSD of an optical element surface generally satisfies the following power-law relationship[21]:

$$S_{\mathrm{ph}}(\theta) = \frac{S_0}{k_x^b}. \tag{6}$$

Referring to the element parameters provided by the NIF device[22], we use the following parameters as the initial PSD distribution of surface distortion of reflective optical elements: $S_0 = 10\ \mathrm{nm}^2 \cdot \mathrm{mm}$; $b = 1.55$, $k_x/2\pi < 1\ \mathrm{mm}^{-1}$; $b = 2.55$, $k_x/2\pi > 1\ \mathrm{mm}^{-1}$. With these parameters, the peak to valley (PV) value of the surface distortion is 60 nm.

When an optical element introduces phase noise into a laser pulse, due to slightly different transmission directions of noise at different spatial frequencies, the phase noise and amplitude noise of the laser will be mutually transformed during transmission in vacuum. However, before the noise leaves the main laser (i.e., self-filtering[23–25]), the power spectrum of the noise remains unchanged. After incident on a transmission element with the Kerr effect, due to the stronger laser intensity positions having a larger refractive index, $n = n_0 + n_2 I$, these positions tend to converge to the surrounding energy, so the laser pulse will change from a uniform distribution to a distribution with some modulation, and the initial noise of the laser pulse will be amplified, that is, the SSSF. The growth multiple of the SSSF is related to the B-integral as follows:

$$\begin{aligned} G = &\left(\cosh^2(\eta B) + \frac{4\Theta^2}{\eta^2}\sinh^2(\eta B)\right)\sin^2\varphi_{\mathrm{in}} \\ &+ \left(\cosh^2(\eta B) + \frac{\eta^2}{4\Theta^2}\sinh^2(\eta B)\right)\cos^2\varphi_{\mathrm{in}} \\ &+ \left(\frac{2\Theta}{\eta} + \frac{\eta}{2\Theta}\right)\cosh(\eta B)\sinh(\eta B)\sin 2\varphi_{\mathrm{in}}, \end{aligned} \tag{7}$$

$$\Theta = \frac{n_0\theta^2}{4n_2|E_0|^2}, \tag{8}$$

$$\eta = 2\sqrt{\Theta - \Theta^2}, \tag{9}$$

where $\theta = k_x/(n_0 k_0)$ is the tilt angle of the noise within the near-field and φ_{in} is the initial phase of the noise.

It can be seen that the growth rate of the SSSF is related to the initial phase φ_{in} of the noise. Since the phase of the noise is usually random when it reaches the Kerr medium, the initial phase can be averaged to obtain the average growth multiple of the SSSF:

$$G_{\mathrm{av}} = 1 + \frac{2}{\eta^2}\sinh^2(\eta B). \tag{10}$$

Considering the self-filtering effect during laser transmission, that is, when the laser is transmitted in the pipe, the noise elements gradually spread out of the laser aperture and are blocked by the edge of the pipe or the downstream optical elements, resulting in a reduction of noise energy. When considering the self-filtering effect, the amplification factor of the noise should be corrected. Let the laser pulse be emitted from the source plane and then propagate freely to the target plane at a distance of L. The visible angle is defined as $\theta_{\mathrm{v}} = w_0/L$, where w_0 is the waist of the laser pulse. Then, the ratio of noise between the source plane and the target plane, that is, the noise transmission rate, is given by the following[25]:

$$T(\theta) = \frac{2}{\pi}\int_0^1 \mathrm{Re}\left(\arccos\left(\frac{(\theta/\theta_{\mathrm{v}})^2 + x^2 - 1}{2x\theta/\theta_{\mathrm{v}}}\right)\right) x\mathrm{d}x. \tag{11}$$

Therefore, the PSD of spatial noise when it reaches the target plane after starting from the noise source plane and then being amplified in the Kerr medium can be expressed as follows:

$$S_{\mathrm{out}}(\theta, B) = T(\theta)\, G_{\mathrm{av}}(\theta, B)\, S_{\mathrm{ph}}(\theta). \tag{12}$$

We take the Nd:glass laser as an example. For phosphate glass, typical parameters are $n_0 = 1.5$, $n_2 = 3.35 \times 10^{-20}\ \mathrm{m}^2/\mathrm{W}$, and saturation energy $E_{\mathrm{s}} = 3.1\ \mathrm{J/cm}^2$. After calculating the PSD of the input and output pulse, we convert the PSD back into random phase noise. Then we multiply this phase noise by a super-Gaussian distributed optical field amplitude and let it freely propagate for a certain distance: $L_{\mathrm{free}} = \frac{\pi c}{2\omega_0 n_2 I} \approx 1$ m; the phase noise is transformed into energy noise with a certain amplitude and phase. A simulation result with a laser intensity of $1\ \mathrm{GW/cm}^2$, a laser diameter of 100 mm (fifth-order super-Gaussian distribution), a self-filtering path length of 1 m and a B-integral of 2 is shown in Figure 3.

We take the PV value of the near-field modulation reaching 1.8 as the criterion to calculate the maximum allowable B-integral under different noise energies S_0. For each case, we conducted 100 simulations and took the average PV value. The calculation results are shown in Figure 4, where the blue, red and yellow lines correspond to the laser intensities of 1, 5 and 10 $\mathrm{GW/cm}^2$, respectively, and the solid and dashed lines correspond to the self-filtering lengths of 1, 10 and 20 m, respectively. It can be seen that for a single standard optical element ($S_0 = 10\ \mathrm{nm}^2 \cdot \mathrm{mm}$), the maximum tolerable B-integral is approximately 2.5, and it slightly increases as the laser intensity increases. Through the self-filtering effect, the maximum B-integral can be increased by 0.1–0.3, and the higher the laser intensity, the more the B-integral increases by the self-filtering effect. This is because when the laser intensity is high, the amplified noise is mainly the high-frequency components, which are more easily filtered

https://doi.org/10.1017/hpl.2025.10033 Published online by Cambridge University Press

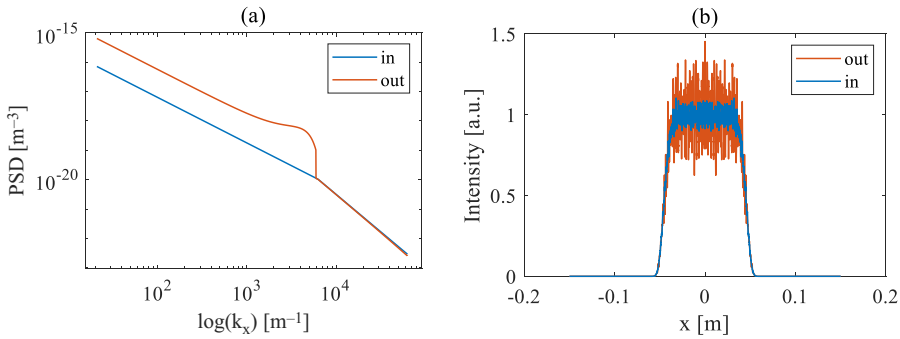

Figure 3. Simulation result of the PSD curves (a) and the intensity distribution (b) of the input pulse (blue solid line) and the output pulse (red solid line) with a laser intensity of 1 GW/cm^2, a laser diameter of 100 mm (fifth-order super-Gaussian distribution), a B-integral of 2 and a self-filtering path length of 1 m.

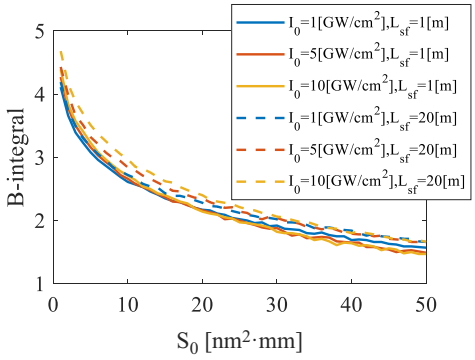

Figure 4. For rectangular-time-profile narrowband Nd:glass lasers, the B-integral required for the near-field modulation to reach 1.8 under different initial noise energies S_0.

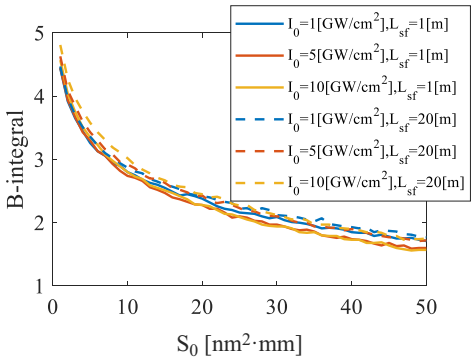

Figure 5. For picosecond Nd:glass lasers, the B-integral required for the near-field modulation to reach 1.8 under different noise energies S_0.

out by self-filtering. When the noise energy reduces to one-quarter of the original, the maximum tolerable B-integral increases to about 3.5. When the noise energy increases to four times the original (i.e., continuously reflected by 16 standard optical elements), the maximum tolerable B-integral decreases to 1.7. It should be noted that the optical path length L required for self-filtering is related to the laser waist w_0. If the laser waist is doubled, to maintain the same viewing angle, the optical path length L also needs to be doubled to achieve the same self-filtering effect.

In the above calculation, only the spatial distribution of the laser pulse was considered. The temporal distribution was not taken into account. That is, it was assumed that the laser had a rectangular distribution in the time domain, and the chirp of the laser pulse can be neglected. With these assumptions, the amplification distribution of the spatial noise at different times is the same. Therefore, the above conclusion is only applicable to narrowband nanosecond pulses that have a rectangular distribution in the time domain. However, for picosecond lasers, although their bandwidth is relatively narrow, the laser pulse often has a Gaussian or Lorentzian distribution in the time domain. In this case, the amplification distribution of the spatial noise at different times is completely different. For femtosecond lasers, the laser pulse has different local frequencies at different times. In this case the amplification distribution of the spatial noise at different times is also different too. We first consider Nd:glass picosecond lasers; let the temporal waveform of the laser pulse be $E(t) \propto \exp\left(-\frac{\ln(2)}{2}\left(2\frac{\omega(t)-\omega_0}{\Delta\omega}\right)^{2n_{SG}}\right)$, $\omega(t) = \frac{C}{T_p^2}t$, $\Delta\lambda = 5$ nm, $n_{SG} = 1$. For each moment within the pulse width, we assume that the phase noise has the same initial distribution, and calculate the final distribution of the noise at each moment. Then we transfer the phase modulation into intensity modulation by letting the laser pulse freely propagate L_{free}. Finally, we accumulate the laser intensities at each moment and calculate the near-field fluence modulation. We calculated the B-integral required for the PV value of the fluence modulation to reach 1.8 under different noise energies, and calculated 100 times for each case and took the average value. The calculation results are shown in Figure 5, where the blue, red and yellow lines correspond to the laser intensities of 1, 5 and 10 GW/cm^2, respectively, and the solid and dashed lines correspond to the self-filtering lengths of 1, 10 and 20 m, respectively. It can be seen that for a single standard optical element, the maximum tolerable B-integral is 2.9. When the noise energy reduces to one-quarter of the original, the maximum tolerable B-integral increases to

https://doi.org/10.1017/hpl.2025.10033 Published online by Cambridge University Press

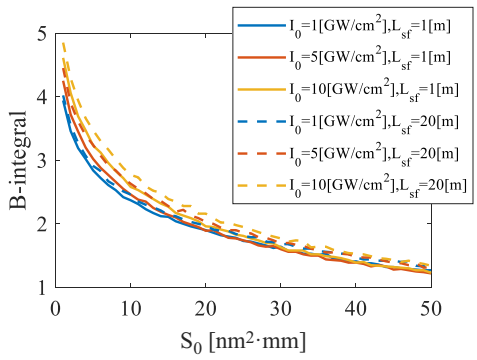

Figure 6. For femtosecond Ti:sapphire lasers, the B-integral required for the near-field modulation to reach 1.8 under different noise energies S_0.

around 3.8; when the noise energy increases to four times the original, the maximum tolerable B-integral decreases to around 1.9. In all three cases, the tolerable B-integral remains basically unchanged as the laser intensity increases. The self-filtering effect can slightly increase the maximum B-integral by 0.1–0.3. Although self-filtering can filter out high-spatial-frequency noise, for the characteristic optical intensity we used in the simulation, a freely propagating length of tens of meters is not sufficient to effectively filter out the SSSF noise.

Next, we consider the case of broadband femtosecond lasers. Taking the Ti:sapphire laser as an example, its specific parameters are $n_0 = 1.76$, $n_2 = 4.77\times10^{-20}$ m^2/W, and saturation energy $E_s = 0.9$ J/cm^2. For broadband lasers, although their spectrum is wide and they often have a rectangular distribution, due to the different instantaneous frequencies at each moment, the SSSF at different moments also has slightly different amplification distributions. Assuming that the parameters of the femtosecond laser are $\Delta\lambda = 40$ nm, $n_{SG} = 4$, and that the laser pulse has the same initial surface distortion at each moment, after the same processing as before, due to the slight difference in local wavelength at each moment, the amplification distributions of noise at different moments will be slightly different, and thus a slightly different final surface distortion will be obtained at each moment. Finally, the surface distortion is converted into wavefront phase distortion, $\varphi(x,y,t) = z(x,y,k_0(t))\cdot k_0(t)$, and the laser pulse is allowed to freely propagate a distance L_{free}. After that, the near-field fluence modulation is calculated (averaged over 100 calculations). We take the fluence modulation reaching 1.8 as the criterion and calculate the B-integral with different intensities. The calculation results are shown in Figure 6. It can be seen that for a single standard optical element, the maximum tolerable B-integral in this case is 2.5, and it slightly increases when the laser intensity increases. When the noise energy reduces to one-quarter of the original, the maximum tolerable B-integral increases to around 3.3, and this value significantly increases when the laser intensity increases. When the noise energy increases to four times the original, the maximum tolerable B-integral decreases to around 1.5, and it remains basically unchanged when the laser intensity increases. Through the self-filtering effect, the maximum B-integral can be increased by 0.1–0.3. Overall, the calculation results of the Ti:sapphire laser in Figure 6 are not much different from those of the rectangular narrowband neodymium glass laser shown in Figure 4. Compared with narrowband lasers, broadband lasers can reduce the fluence modulation caused by the SSSF through the spectral smoothing effect, and thus the tolerable B-integral can be increased. However, because the wavelength of the Ti:sapphire laser is shorter than the wavelength of the Nd:glass laser, the same surface distortion of optical elements means a larger wavefront phase distortion for the Ti:sapphire laser, which offsets the benefits brought by the spectral smoothing effect.

In the development of Beamlet (a nanosecond Nd:glass laser system as the prototype of NIF architecture), researchers found that the maximum value of B-integral should not be larger than 1.8 to avoid severe near-field modulation caused by the SSSF[15], which was consistent with our numerical results. In the design of picosecond and femtosecond laser systems, this criterion was adopted despite some researches[17,18] suggesting that this criterion can be relaxed. We find that this is true for picosecond Nd:glass laser systems; for femtosecond Ti: sapphire laser systems we need to consider the number of optical components in the system, which was usually less than in the Nd:glass laser systems.

4. Influence of the B-integral on laser focusability

Other than causing the SSSF in the near-field, the B-integral also induces wavefront phase distortion, which does not increase the intensity modulation in the near-field, but will degenerate the focal spot in the far-field. The transmission or reflection spatial filter can suppress the growth of the laser intensity modulation in the near-field and protect the optical elements from laser damage. The wavefront phase distortion can also be compensated by a deformable mirror. However, this compensation is not perfect. The laser intensity profile varies at different moments, causing different wavefront phase distortions at different moments, but the deformable mirror can only compensate for the wavefront phase distortion at a certain moment. Besides, the unit size of the deformable mirror is limited, which means it can only compensate for the phase distortion in the low-spatial-frequency region. In this section, we use the (time-integrated) Strehl ratio of the far-field as the standard to calculate the influence of the B-integral on the laser focusing capability under different cases, and accordingly provide the B-integral criterion for broadband lasers. The specific calculation method is as follows: assume the central wavelength of the laser is 1 μm. For the amplitude noise of a laser

https://doi.org/10.1017/hpl.2025.10033 Published online by Cambridge University Press

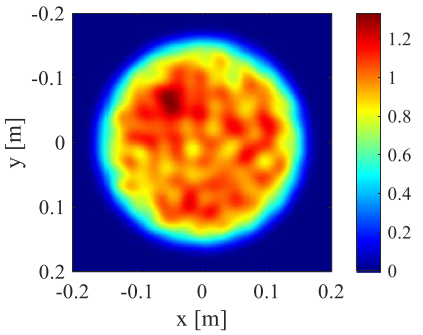

Figure 7. Spatial intensity distribution generated by the simulation program.

electric field, its PSD can be approximately described by Equation (6). To simulate the filtering effect of the spatial filter, we ignore the intermediate and high-frequency parts of the PSD function and generate a spatial intensity distribution using the low-frequency part with a wave number less than $2\pi \times 0.03\ \mathrm{mm}^{-1}$, which cannot be filtered out by the pinhole of spatial filters. We increase the laser diameter to 300 mm (fifth-order super-Gaussian distribution) to better simulate the low-frequency distortion, with a step size of $\mathrm{d}x = \mathrm{d}y = 2$ mm. A spatial intensity distribution generated by the above method is shown in Figure 7.

After generating the spatial distribution, in the temporal domain, we set the laser profile as a chirped laser pulse with an n_{SG}-order super-Gaussian distribution. After passing through the Kerr medium, the laser accumulates a certain value of the B-integral. The laser pulse is then compressed back to the transform limit, and a phase compensation is given to the laser pulse through a deformable mirror. Theoretically, the phase to be compensated by the deformable mirror should be the phase of the compressed laser at the moment of the highest intensity, which can achieve the best compensation effect. However, in actual experiments, this phase cannot be measured. Therefore, we choose the phase distribution at the central wavelength of the laser pulse before compression as the phase to be compensated by the deformable mirror[24]. The unit sizes of the deformable mirror are 10, 20 and 30 mm, respectively. For a broadband laser pulse under the paraxial approximation, the far-field fluence distribution $F_{\mathrm{f}}(x_{\mathrm{f}},y_{\mathrm{f}})$ at the focal plane after passing through an ideal lens can be calculated through the Fresnel–Kirchhoff integral[26]:

$$S_0(\omega, x_0, y_0) = \frac{1}{\sqrt{2\pi}} \int E(t, x_0, y_0)\, e^{-i\omega t} \mathrm{d}t, \tag{13}$$

$$S_{\mathrm{f}}(\omega, x_{\mathrm{f}}, y_{\mathrm{f}}) = \frac{-ik(\omega)}{2\pi f} e^{-ik(\omega)f - ik(\omega)\frac{x_{\mathrm{f}}^2 + y_{\mathrm{f}}^2}{2f}} \iint S_0(\omega, x_0, y_0)\, e^{ik(\omega)\frac{x_0 x_{\mathrm{f}} + y_0 y_{\mathrm{f}}}{f}} \mathrm{d}x_0 \mathrm{d}y_0, \tag{14}$$

$$F_{\mathrm{f}}(x_{\mathrm{f}}, y_{\mathrm{f}}) = \int |S_{\mathrm{f}}(\omega, x_{\mathrm{f}}, y_{\mathrm{f}})|^2 \mathrm{d}\omega. \tag{15}$$

The values of $F_{\mathrm{f}}(0,0)$ in the far-field focal spot with a certain value of the B-integral and without B-integral are calculated respectively, and the ratio of the two is the (time-integrated) Strehl ratio. The calculation results of the Strehl ratio under different B-integrals and different deformable mirror unit sizes are shown in Figure 8. We take the Strehl ratio decreasing to 0.8 as the maximum tolerable B-integral. It can be seen that when the laser bandwidth is 5, 10, 20 and 40 nm, the maximum tolerable B-integral without a deformable mirror is 2.2, 1.9, 1.8 and 1.7, respectively. After adding a deformable mirror with a unit size of 30 mm, the maximum tolerable B-integral increases to 3.2, 3.7, 3.9 and 4, respectively. When the unit size of the deformable mirror is 20 mm, the maximum tolerable B-integral further increases to 3.6, 4.7, 5.2 and 5.4, respectively. When the unit size of the deformable mirror is 10 mm, the maximum tolerable B-integral is 4.4, more than 6, more than 6 and more than 6, respectively. If the deformable mirror is not installed, the Strehl ratio decreases more severely when the B-integral increases for wider laser bandwidths and larger n_{SG}. This is because the leading and trailing edges of broadband lasers with larger n_{SG} have higher intensities, and under the same B-integral, the leading and trailing edges accumulate larger nonlinear phase shifts, thus having more severe wavefront phase distortions. However, after adding a deformable mirror, the Strehl ratio of the laser pulse shows a significant improvement. Moreover, the wider the laser bandwidth and the larger the n_{SG}, the better the correction effect of the deformable mirror. This is because before compression, the temporal profile of a broadband laser is closer to a rectangular pulse with larger n_{SG}, which enhances the correction effect of the deformable mirror. For the considered laser bandwidth range, using a deformable mirror with a unit size of 30 mm can achieve a satisfactory improvement in the Strehl ratio.

The criterion that the total B-integral of the system must be less than 3.5 to ensure wavefront distortion does not degrade laser far-field focusing capability originates from LLNL's simulation[16] of transmission and focal spot of fundamental (1ω) and third harmonic (3ω) waves under 1 ns square pulse. After the LLNL established these criteria, subsequent designs of similar systems adopted them as a standard. However, the LLNL's simulations had several limitations. Firstly, the LLNL did not use an authentic low-frequency wavefront model. Instead, an artificially constructed Gaussian random phase model was employed. Secondly, the simulation assumed a simplified deformable mirror capable of perfectly correcting all low-frequency wavefront aberrations, which is unrealistic in practical systems. Thirdly, the simulations were restricted to nanosecond square pulses and do not generalize to picosecond or femtosecond pulse scenarios. In our simulations, we utilized a more realistic low-frequency phase model and a deformable mirror model. Our simulation results are applicable not only to nanosecond pulses but also

https://doi.org/10.1017/hpl.2025.10033 Published online by Cambridge University Press

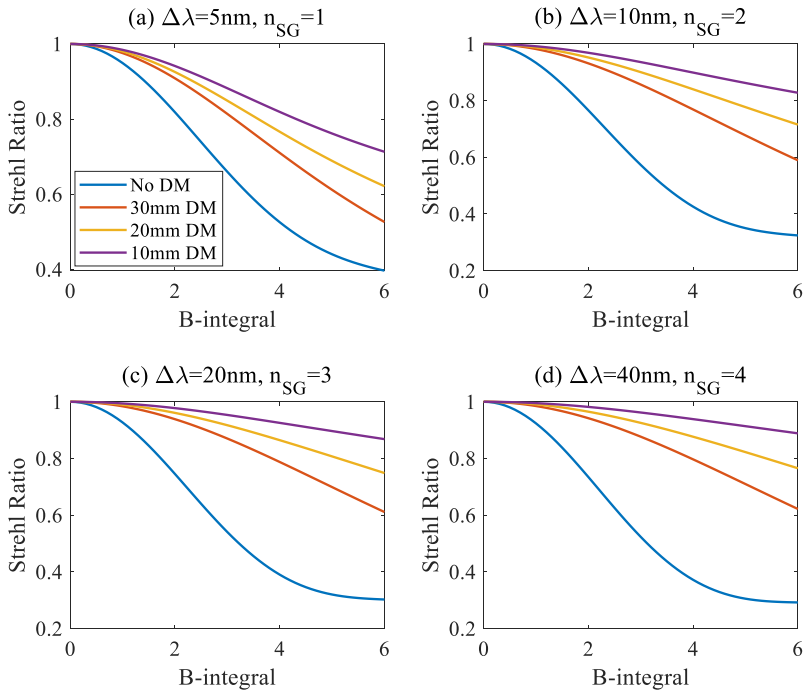

Figure 8. The variation of the Strehl ratio in the far-field with the B-integral under different laser bandwidths, temporal super-Gaussian orders and deformable mirror element sizes (no deformable mirror, 10 mm, 20 mm and 30 mm).

to picosecond and femtosecond pulses, providing design criteria for the upper limit of the total B-integral in nanosecond, picosecond and femtosecond laser systems.

5. Conclusion

In the design and construction of ultra-high-peak-power laser systems, the control of the B-integral has always been an important factor to consider when formulating system schemes and selecting element parameters. The influence of the B-integral on ultra-high-peak-power lasers is mainly manifested in three aspects: in the time domain, the introduction of the B-integral leads to the generation of high-order dispersion terms, affecting the compression effect of the laser pulse; in the spatial domain, on the one hand, the introduction of the B-integral causes the laser pulse to have a wavefront phase distortion, thereby affecting the far-field focusability of the laser; on the other hand, the growth rate of the SSSF in the laser pulse is directly related to the B-integral. Currently, there is no strict B-integral criterion for broadband picosecond and femtosecond lasers. The results of the B-integral criterion for nanosecond lasers are usually directly applied to picosecond and femtosecond lasers, which is inappropriate. In this paper, the impact of the B-integral on the output capability of broadband laser systems is evaluated using the intensity decease caused by SPM, the near-field intensity modulation caused by the SSSF and the far-field Strehl ratio as indicators. In the calculation of near-field modulation, Nd:glass lasers and Ti:sapphire lasers were taken as typical examples of picosecond and femtosecond laser systems, respectively. For picosecond lasers, the SPM effect and the SSSF limit the maximum tolerable B-integral. SPM limits the maximum tolerable B-integral to around 1.7, while the SSSF limits the maximum tolerable B-integral to around 1.9. For femtosecond lasers, the value of the B-integral is mainly limited by the SSSF and the far-field Strehl ratio. The SSSF limits the maximum tolerable B-integral to around 1.5. If the SSSF is suppressed by reducing the number of optical elements or decreasing the surface distortion of the optical elements, the limitation on the B-integral can be relaxed to around 2.5. Within the studied parameter range, the self-filtering effect has a relatively small impact on the maximum B-integral, and only when the laser intensity is relatively high can the self-filtering effect significantly increase the maximum B-integral. For picosecond or femtosecond lasers, the far-field focusability limits the B-integral to 2.2 or 1.7, which is a strong restriction. However, this restriction can be largely relaxed by inserting a deformable mirror. The study of the B-integral will provide guidance for the design of ultra-high-peak-power laser systems.

Funding

This research is supported by the National Key Laboratory of Plasma Physics Fund (Nos. 6142A04220204 and 6142A04230303), the Independent Research Project of the National Key Laboratory of Plasma Physics (Nos. JCKYS2023212802 and JCKYS2024212806) and the

https://doi.org/10.1017/hpl.2025.10033 Published online by Cambridge University Press

National Key Research and Development Program of China (No. 2022YFB3606305).

References

1. D. Strickland and G. Mourou, Opt. Commun. **56**, 219 (1985).
2. D. Doria, M. O. Cernaianu, P. Ghenuche, D. Stutman, K. A. Tanaka, C. Ticos, and C. A. Ur, J. Instrum. **15**, C09053 (2020).
3. D. M. Pennington, M. D. Perry, B. C. Stuart, R. D. Boyd, J. A. Britten, C. G. Brown, S. M. Herman, J. L. Miller, H. T. Nguyen, B. W. Shore, G. L. Tietbohl, and V. P. Yanovsky, Proc. SPIE **3047**, 490 (1997).
4. C. N. Danson, P. A. Brummitt, R. J. Clarke, J. L. Collier, B. Fell, A. J. Frackiewicz, S. Hancock, S. Hawkes, C. Hernandez-Gomez, P. Holligan, M. H. R. Hutchinson, A. Kidd, W. J. Lester, I. O. Musgrave, D. Neely, D. R. Neville, P. A. Norreys, D. A. Pepler, C. J. Reason, W. Shaikh, T. B. Winstone, R. W. W. Wyatt, and B. E. Wyborn, Nucl. Fusion **44**, 239 (2004).
5. Y. Kitagawa, H. Fujita, R. Kodama, H. Yoshida, S. Matsuo, T. Jitsuno, IEEE J. Quantum Electron. **40**, 281 (2004).
6. J. M. Di Nicola, S. T. Yang, C. D. Boley, J. K. Crane, J. E. Heebner, T. M. Spinka, P. Arnold, C. P. J. Barty, M. W. Bowers, T. S. Budge, K. Christensen, J. W. Dawson, G. Erbert, E. Feigenbaum, G. Guss, C. Haefner, M. R. Hermann, D. Homoelle, J. A. Jarboe, J. K. Lawson, R. Lowe-Webb, K. P. McCandless, B. McHale, L. J. Pelz, P. P. Pham, M. A. Prantil, M. L. Rehak, M. A. Rever, M. C. Rushford, R. A. Sacks, M. Shaw, D. Smauley, L. K. Smith, R. Speck, G. Tietbohl, P. J. Wegner, and C. Widmayer, Proc. SPIE **9345**, 93450I (2015).
7. E. W. Gaul, M. Martinez, J. Blakeney, A. Jochmann, M. Ringuette, D. Hammond, T. Borger, R. Escamilla, S. Douglas, W. Henderson, G. Dyer, A. Erlandson, R. Cross, J. Caird, C. Ebbers, and T. Ditmire, Appl. Opt. **49**, 1676 (2010),
8. N. Blanchot, G. Behar, J. C. Chapuis, C. Chappuis, S. Chardavoine, J. F. Charrier, H. Coïc, C. Damiens-Dupont, J. Duthu, P. Garcia, J. P. Goossens, F. Granet, C. Grosset-Grange, P. Guerin, B. Hebrard, L. Hilsz, L. Lamaignere, T. Lacombe, E. Lavastre, T. Longhi, J. Luce, F. Macias, M. Mangeant, E. Mazataud, B. Minou, T. Morgaint, S. Noailles, P. Patelli, E. Perrot-Minnot, C. Present, B. Remy, C. Rouyer, N. Santacreu, M. Sozet, D. Valla, and F. Laniesse, Opt. Express **25**, 16957 (2017).
9. W. P. Leemans, J. Daniels, A. Deshmukh, A. J. Gonsalves, A. Magana, H. S. Mao, D. E. Mittelberger, K. Nakamura, J. R. Riley, D. Syversrud, C. Toth, and N. Ybarrolaza, in *Proceedings of PAC2013* (2013), paper THYAA1.
10. J. H. Sung, H. W. Lee, J. Y. Yoo, J. W. Yoon, C. W. Lee, J. M. Yang, Y. J. Son, Y. H. Jang, S. K. Lee, and C. H. Nam, Opt. Lett. **42**, 2058 (2017).
11. W. Li, Z. Gan, L. Yu, C. Wang, Y. Liu, Z. Guo, L. Xu, M. Xu, Y. Hang, Y. Xu, J. Wang, P. Huang, H. Cao, B. Yao, X. Zhang, L. Chen, Y. Tang, S. Li, X. Liu, S. Li, M. He, D. Yin, X. Liang, Y. Leng, R. Li, and Z. Xu, Opt. Lett. **43**, 5681 (2018).
12. C. Radier, O. Chalus, M. Charbonneau, S. Thambirajah, G. Deschamps, S. David, J. Barbe, E. Etter, G. Matras, S. Ricaud, V. Leroux, C. Richard, F. Lureau, A. Baleanu, R. Banici, A. Gradinariu, C. Caldararu, C. Capiteanu, A. Naziru, B. Diaconescu, V. Iancu, R. Dabu, D. Ursescu, I. Dancus, C. A. Ur, K. A. Tanaka, and N. V. Zamfir, High Power Laser Sci. Eng. **10**, e21 (2022).
13. X. Zeng, K. Zhou, Y. Zuo, Q. Zhu, J. Su, X. Wang, X. Wang, X. Huang, X. Jiang, D. Jiang, Y. Guo, N. Xie, S. Zhou, Z. Wu, J. Mu, H. Peng, and F. Jing, Opt. Lett. **42**, 2014 (2017).
14. C. N. Danson, C. Haefner, J. Bromage, T. Butcher, J.-C. F. Chanteloup, E. A. Chowdhury, A. Galvanauskas, L. A. Gizzi, J. Hein, D. I. Hillier, N. W. Hopps, Y. Kato, E. A. Khazanov, R. Kodama, G. Korn, R. Li, Y. Li, J. Limpert, J. Ma, C. H. Nam, D. Neely, D. Papadopoulos, R. R. Penman, L. Qian, J. J. Rocca, A. A. Shaykin, C. W. Siders, C. Spindloe, S. Szatmári, R. M. G. M. Trines, J. Zhu, P. Zhu, and J. D. Zuegel, High Power Laser Sci. Eng. **7**, e54 (2019).
15. P. Wegner and S. Burkhart, Inertial Confinement Fusion **9**, 44 (1998).
16. W. H. Williams and J. M. Auerbach, in *3rd International Conference on Solid-state Lasers for Applications to Inertial Confinement Fusion* (1998), p. 22.
17. J. Zhang, S. Wen, X. Fu, L. Zhang, J. Deng, and D. Fan, Proc. SPIE **7843**, 78431T (2010).
18. E. A. Khazanov, Quantum Electron. **52**, 208 (2020).
19. I. N. Ross, P. Matousek, G. H. C. New, and K. Osvay, J. Opt. Soc. Am. B **19**, 2945 (2002).
20. V. I. Bespalov and V. I. Talanov, JETP Lett. **3**, 307 (1996).
21. V. N. Ginzburg, A. A. Kochetkov, S. Yu. Mironov, A. K. Potemkin, D. E. Silin, and E. A. Khazanov, Radiophys. Quantum Electron. **62**, 849 (2020).
22. M. L. Spaeth, K. R. Manes, C. C. Widmayer, W. H. Williams, P. K. Whitman, M. A. Henesian, I. F. Stowers, and J. Honig, Opt. Eng. **43**, 2854 (2004).
23. S. Mironov, V. Lozhkarev, G. Luchinin, A. Shaykin, and E. Khazanov, Appl. Phys. B. **113**, 147 (2013).
24. V. N. Ginzburg, A. A. Kochetkov, A. K. Potemkin, and E. A. Khazanov, Quantum Electron. **48** 325 (2018).
25. V. N. Ginzburg, A. A. Kochetkov, S. Yu. Mironov, A. K. Potemkin, D. E. Silin, and E. A. Khazanov, Radiophys. Quantum Electron. **62**, 849 (2020).
26. M. Martyanov, S. Mironov, M. Starodubtsev, A. Soloviev, A. Kochetkov, V. Ginzburg, A. Shaikin, and E. Khazanov, J. Opt. Soc. Am. B **39**, 1936 (2022).

https://doi.org/10.1017/hpl.2025.10033 Published online by Cambridge University Press